Impact of Iron Incorporation on 2-4 nm Size Silicon Nanoparticles Properties.

Juan J. Romero,[a] Marc Wegmann,[c] Hernán B. Rodríguez,[a] Cristian Lillo,[a] Aldo Rubert,[a] Stefanie Klein,[c] Mónica L. Kotler,[b] Carola Kryschi,[c] Mónica C. Gonzalez.[a*]

[a] *Instituto de Investigaciones Fisicoquímicas Teóricas y Aplicadas (INIFTA), Facultad de Ciencias Exactas, Universidad Nacional de La Plata, Casilla de Correo 16, Sucursal 4, (1900) La Plata, Argentina.*

[b] *IQUIBICEN-CONICET, Departamento de Química Biológica, Facultad de Ciencias Exactas y Naturales, Universidad de Buenos Aires, Argentina.*

[c] *Department Chemistry and Pharmacy, Physical Chemistry I and ICMM, Friedrich-Alexander University of Erlangen-Nuremberg, Egerlandstr. 3, D-91058 Erlangen, Germany.*

✉ *E-mail:* gonzalez@inifta.unlp.edu.ar ;TE: 54-221-4257291 / 4257430; FAX: 54-221- 4254642

ABSTRACT

Iron-containing silicon nanoparticles were synthesized in an attempt to understand the effect of iron on the silicon nanoparticle (SiNP) photoluminescence and singlet-oxygen generation capacity. A wet chemical oxidation procedure of the sodium silicide precursor, obtained from the thermal treatment in anaerobic conditions of a mixture of sodium, silicon, and an iron (III) organic salt under anaerobic conditions, was employed. Surface-oxidized and propylamine-terminated SiNPs were characterized using high-resolution transmission electron microscopy, X-ray photoelectron spectroscopy, time-resolved and steady-state photoluminescence, and time-correlated fluorescence anisotropy. Based on differences in the morphology, crystal structure, density, and photoluminescence spectrum, two distinct types of SiNPs were identified in a given synthesis batch: iron-free and iron-containing SiNPs. The results show that iron is inhomogeneously incorporated in the SiNPs leading to an efficient photoluminescence quenching. Emission arrives mainly from 2 nm size iron-free SiNPs. The nanoparticles were shown to generate singlet oxygen ($^1O_2$) upon 355 nm irradiation, though they were able to quench $^1O_2$. Analysis of cytotoxicity using MTT assay on rat glioma C6 cells showed a strong dependence on the nature of the surface groups, as 100 μg/ml of propylamine-terminated iron-containing SiNPs leads to 85% decrease in cell viability while equal amounts of surface oxidized particles induced a 35% of cell death.

Keywords: iron quenching, optical properties, surface chemistry, singlet oxygen.

INTRODUCTION

Luminescent silicon nanoparticles (SiNPs) of 1-5 nm size were shown to offer the potential to significantly improve existing methods of cancer diagnosis and treatment as alternative materials for organic dyes and toxic cadmium-based nanoparticles due to their high photoluminescence quantum yields, high photostability in aqueous solution and ambient air, good biocompatibility and tunable surface functionalization for drug delivery. Moreover, SiNPs are composed of nontoxic Si and thus, have little environmental impact. These properties enable SiNPs to be used as real-time *in vivo* imaging agents. Another important property of SiNPs is their capability for singlet oxygen ($^1O_2$) and superoxide ($O_2^{\cdot-}$) generation.[1, 2]

Among the different formulations that enhance SiNPs potential for nano-oncology applications, the synthesis of magnetic SiNPs may allow for magnetic-field guided tumor tissue targeting in combination with optical imaging as well as $^1O_2$ and $O_2^{\cdot-}$ generation. Different strategies were reported in the literature for the design of such bimodal imaging agents. Magnetic iron silicide nanowires on crystalline silicon were among the first reported materials with such characteristics.[3] Another approach consisted in the co-encapsulation of luminescent silicon quantum dots and superparamagnetic iron oxide nanoparticles within the hydrophobic core of biocompatible phospholipid − polyethyleneglycol (DSPE-PEG) micelles, which showed an enhanced *in vitro* cellular uptake in the presence of magnetic fields.[4] Further approaches involved the combination in a single particle of silicon semiconductor materials with iron oxides[5] and the synthesis of iron-doped silicon nanoparticles obtained from iron-doped sodium silicide precursors ($xFe:Na_4Si_4$).[6] The latter authors reported an extreme loss of photoluminescence with increasing iron dopant concentrations in the initial mixture.

Herein, we investigate the effect of iron on the photoluminescence, singlet oxygen generation, and cytotoxicity towards rat glioma C6 cells of iron-containing SiNPs (Fe-SiNPs) in an attempt to further understand the potential use of these particles as optical sensors and therapeutic agents in biological systems. To that purpose, Fe-SiNPs were synthesized from a modified procedure of the iron-doped sodium silicide precursor reported in the literature.[6] The SiNPs were either surface oxidized or derivatized by silylation to yield Fe-SiNPs with either $-SiO^-$ and $-NH_2$ terminal groups, respectively.

EXPERIMENTAL

Materials. Toluene (99.7%, H_2O 0.005%), methanol, cyclohexane, 9, 10-diphenylanthracene (DPA, 97%), sodium (Na 95%), silicon powder (Si, 99%), anhydrous iron(III) acetylacetonate ($Fe(acac)_3$, 99.99%), allylamine ($C_3H_5NH_2$, 98%), ammonium bromide (NH_4Br, 99.99%), N,N-dimethylformamide (DMF, 99.8%), 3-(4,5-dimethylthiazol-2-yl)-2,5-diphenyltetrazolium bromide (MTT, 98%), and dimethylsulfoxide (DMSO, 99.9%) were purchased from Sigma-Aldrich and employed without further purification. Deionized water (>18 MΩcm, < 20 ppb of organic carbon) was obtained using a Millipore system. Nitrogen (4 bands quality) and oxygen gas were both from La Oxígena S.A., Argentina.

Equipment. FTIR spectra were obtained with a Bruker EQUINOX spectrometer. KBr disks were used as holders. Spectra were taken in the 4000-400 cm^{-1} range with 1 cm^{-1} resolution.

The attenuation spectra were recorded with a double-beam Shimadzu UV-1800 spectrophotometer in a 1 cm quartz cuvette at a scan rate of 300 nm/min. Diffuse transmittance spectra were recorded with a double-beam PGI-T90+ UV-vis spectrophotometer equipped with a $BaSO_4$ integrating sphere in a 0.1 cm quartz cuvette,

and compared to attenuation spectra in order to evaluate possible spectral distortions due to scattering.

PL measurements were performed with a Jobin-Yvon Spex Fluorolog FL3-11 spectrometer. The fluorimeter is equipped with a 450 W Xe lamp as the excitation source, a monochromator with 1 nm bandpass gap for selecting the excitation and emission wavelengths, and a red sensitive R928 PM as detector. All spectra were corrected for the wavelength-dependent sensitivity of the detector and the source. Additionally, the PL spectra were corrected for Raman scattering by using the associated solvent emission spectrum. To estimate the PL emission quantum yield (Φ), the PL emission spectra were collected for various excitation wavelengths. Identical measurements (excitation conditions, lamp energy, and spectrometer band-pass) were performed on 9, 10- diphenylanthracene in cyclohexane, used as reference for PL quantum yield determinations.[7] The temperature was controlled to ± 0.1 ^{o}C with an F-3004 Peltier sample cooler controlled by a LFI-3751 temperature controller (Wavelength electronics). For time-resolved PL measurements the Jobin-Yvon Spex Fluorolog FL3-11 spectrometer (*vide supra*), equipped for time-correlated single photon counting (TCSPC) measurements with LED excitation at 341 and 388 nm (FWHM ~ 400 ps), was used. Data was globally fitted as a sum of exponentials including IRF deconvolution until optimal values of χ^2, residuals, and standard deviation parameters were attained.

TEM micrographs were taken with a Zeiss EM900 instrument operated at 80kV accelerating voltage. Images were analyzed employing the Image Tool 3.0 software (Health Science Center of the University of Texas, San Antonio, USA). Silicon nanoparticles size were determined assuming that the SiNP area obtained from the HR-

TEM images is the projection of a spherical particle. A log-normal function was found to best describe the size distribution of the 500 nanoparticle sample.

Gel electrophoresis was performed using a 1% agarose gel in TAE buffer of pH 8 as support and a TAE buffer of pH 8 as moving phase. The electrophoresis was run for 30 minutes at an applied constant voltage of 100 V. The nanoparticles were detected by their photoluminescence upon irradiation with UV light filtered with a SW06 filter from a G-Box, Synoptics Ltd. Cambridge.

X-ray photoelectron spectroscopy (XPS) measurements were performed using a non-monochromatic Mg K α source (XR50, Specs GmbH) and a hemispherical electron energy analyzer (PHOIBOS 100, Specs GmbH) operating at 40 eV pass energy. A two-point calibration of the energy scale was performed using sputtered cleaned gold (Au 4f7/2, binding energy (BE) = 84.00 eV) and copper (Cu 2p3/2, BE = 932.67 eV) samples. C 1s at 284.6 eV was used as charging reference.

The silicon content in the suspensions was determined by Inductively-Coupled Plasma Atomic Emission Spectroscopy (ICP- AES).

Time-resolved singlet oxygen phosphorescence detection was performed by irradiating the SiNP suspension with a Nd:YAG Surelite II Continuum laser (7 ns FWHM and 14 mJ per pulse at 355 nm). The phosphorescence emission at 1270 nm due to the transition from the lowest excited singlet state to the ground triplet state of molecular oxygen was detected at right angles using an amplified Judson J 116/8sp germanium detector. Because our experimental setup is not able to detect traces below the 5 μs time range, $^1O_2$ emission in either toluene or D_2O (lifetime τ_Δ = 29 and 68 μs,[8] respectively) were used as solvent.

Bilinear Regression Analysis. For low chromophore absorbance (<0.05), the bilinear regression analysis takes advantage of the linearity of the steady-state PL

emission intensity at the given emission wavelength, I(λ_{em}), with both, the absorption coefficient of the fluorophore, $\varepsilon(\lambda_{ex})$, and the factor F($\lambda_{em}$) reflecting the shape of the emission spectrum to retrieve information from the experimental excitation-emission matrix on the minimum number of species and on their relative emission and absorption spectra.[9]

Silicon Nanoparticles Synthesis. A mixture of Na and Si with a mass ratio of 2.27:1 was crushed and carefully mixed for 20 minutes using a mortar and pestle in a N_2-filled glovebox. The powders are oxygen-sensitive, and extreme precautions were taken to avoid exposure to oxygen. The final powder was introduced into a quartz tube placed in a tube furnace and heated at 420 °C for 72 hours under flowing nitrogen. The obtained solid was then poured into a degassed NH_4Br (80 mM) solution in *N*,*N*-dimethylformamide (DMF) and further refluxed for 24 h under N_2 atmosphere. The liquid supernatant contained H-terminated SiNPs. Further steps involved two different procedures to obtain either SiO_x surface oxidized (SiO_x-SiNPs) or propylamine-terminated SiNPs (PA-SiNPs). Surface oxidation was obtained upon two days of gentle heating in air saturated aqueous suspensions. PA-SiNPs involve allylamine addition to freshly prepared SiNPs in cyclohexane followed by 2 h reflux and/or 5 h room temperature photolysis with light of 254 nm from eight Rayonet Lamps (RPR2537A, Southerm N.E. UltravioletCo.). The orange-yellow supernatant contains propylamine-terminated SiNPs. Dried SiO_x-SiNPs and PA-SiNPs were obtained by solvent evaporation in vacuum at < 343 K. The SiNPs were re-suspended in pure water and further purified for water soluble impurities by dialysis.

A similar synthesis procedure was performed to obtain iron-containing silicon nanoparticles, SiO_x-Fe-SiNPs and PA-Fe-SiNPs. To that purpose, a mass ratio Na:Si:Fe(acac)$_3$ of 34.8:15:1 was used for preparing the initial powder (*vide supra*),

corresponding to a molar ratio Si:Fe of 190:1. Scheme 1 shows an outline of the particles synthesis. All the nanoparticles, PA-SiNPs, SiO_x-Fe-SiNPs, SiO_x-SiNPs and PA-Fe-SiNPs form stable aqueous suspensions.

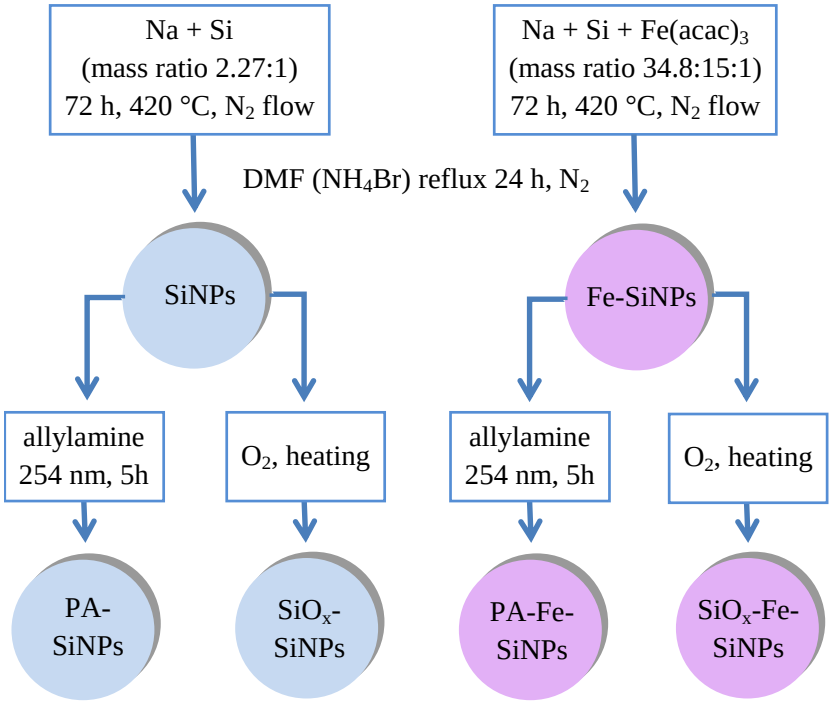

Scheme 1: Summary flow chart of the synthesis pathways followed for obtaining the different SiNPs.

Cell culture and treatments: Rat glioma C6 cells (ATCC CCL-107TM) were maintained in DMEM medium supplemented with 10% heat-inactivated FBS, 2 mM glutamine, 100 U/mL penicillin, 100 µg/mL streptomycin, and 2.5 µg/mL amphotericin B. Cells were cultured on 60-mm plastic dishes at 37 °C under a humidified atmosphere of 5% CO_2 – 95% air and the medium was renewed three times a week. For further uses, C6 cells were removed from Petri dishes with 0.25% trypsin, diluted with DMEM/10% FBS and replated in 96 well-plates to yield 70–80% confluent cultures. Then, cells were washed with phosphate-buffered saline solution (PBS) and used for exposure studies. For this purpose, aliquots of aqueous stock of SiNPs suspensions were

diluted in DMEM/10% SFB to a variable final concentration of 10, 50, 75 and 100 μg/ml and incubated with the cells for 24 h.

Cell viability (MTT assay): After 24 h of incubation, the culture medium was discarded and each well washed twice with PBS. The MTT solution was added to each well to a final concentration of 0.125 mg/ml in culture media. After 1.5 h of incubation, MTT solution was discarded and formazan solubilized in 200 mL of DMSO. Absorbance was measured at 570 nm with background subtraction at 655 nm in a BIO-RAD Model 680 Benchmark microplate reader (BIO-RAD laboratories, Hercules, CA, USA). The MTT reduction activity was expressed as a percentage of the control cells.

RESULTS AND DISCUSSION

Iron-containing and iron-free H-terminated silicon nanoparticles, SiNPs and Fe-SiNPs, were obtained in the laboratory by a modified procedure reported in the literature involving sodium silicide precursors and their further reaction with NH_4Br in DMF.[6] Silicon nanoparticles were either surface oxidized to SiO_x upon aging in air-saturated aqueous suspensions to yield SiO_x-SiNPs and SiO_x-Fe-SiNPs, or surface modified to obtain propylamine-terminated particles, PA-SiNPs and PA-Fe-SiNPs.

Silicon Nanoaparticles Characterization: The analysis of the HR-TEM images of SiO_x-SiNPs in Figure 1A results in an average size of 3.75 ± 0.5 (see histogram in Figure 1C) and a mean spacing between the lattice fringes of 2.9 ± 0.1 Å. The latter spacing is in agreement with that reported for the (111) planes of SiNPs.[5] On the other hand, SiO_x-Fe-SiNPs micrographs (Figure 1B) show two distinct kind of crystals which could be easily discriminated by their contrast, average size and lattice spacing. The low-contrast, 3.75 ± 0.5 nm size SiNPs with a lattice spacing of 2.9 Å resemble SiO_x-SiNPs (light blue box in Figure 1B). On the other hand, the well dispersed, high density, 4.75 ± 0.5 nm average size SiNPs with a lattice spacing of 2.1 ± 0.1 Å (pink box in

Figure 1B) were assigned to Fe-containing SiNPs. Lattice fringe spacing of 1.9 Å were reported for the (220) silicon plane in Fe-doped SiNPs.[6] However, the lattice spacing of 2.1–2.0 Å is also consistent with the (400) spacing in cubo-octahedral morphologies of botanical magnetites.[10, 11] The larger mean diameters observed for the Fe-containing particles are in line with literature reports associating increasing average sizes for SiNPs with rising Fe content.[5] In consequence, TEM images strongly support that synthesis batches of SiO_x-Fe-SiNPs, are actually an intimate mixture of iron-free and iron-containing particles.

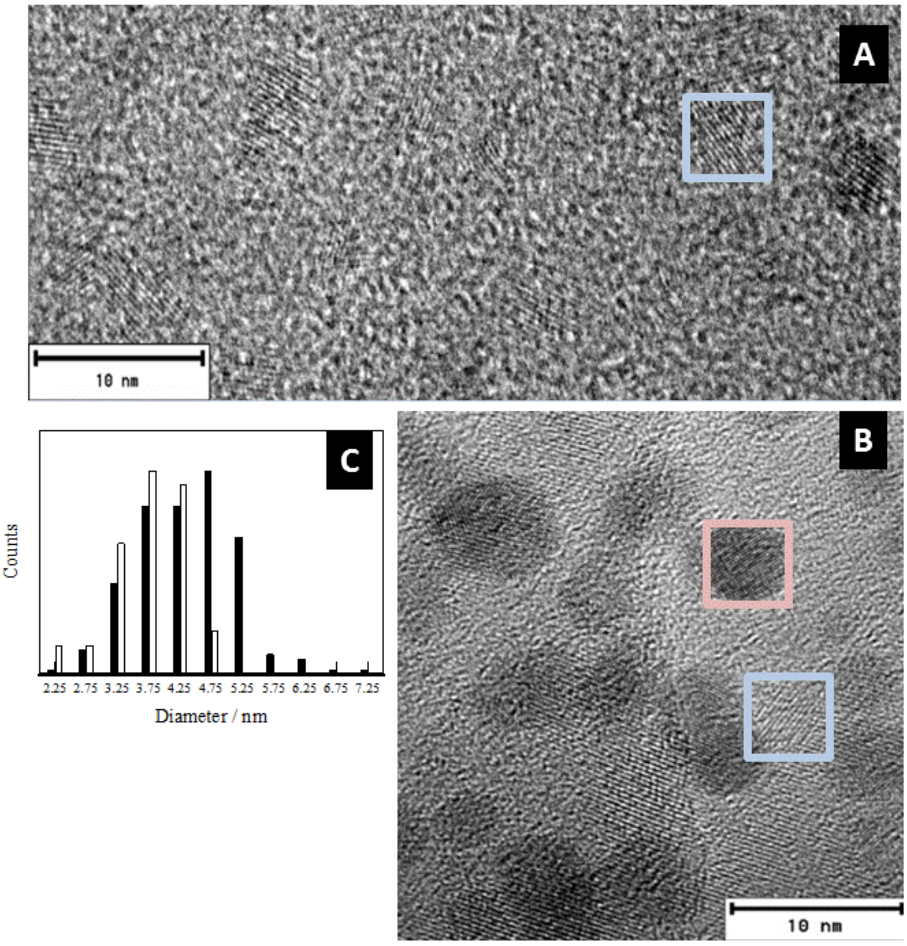

Figure 1: HR-TEM images of (A) SiO_x-SiNPs, (B) SiO_x-Fe-SiNPs, and (C) associated size histogram of 500 well-dispersed SiO_x-SiNPs (white bars) and SiO_x-Fe-

SiNPs (black bars). Light blue and pink boxes show SiO_x-SiNPs and an iron-containing SiO_x-SiNP, respectively.

The XPS of SiO_x-Fe-SiNPs (see Figure 2) shows the characteristic Si 2s, Si 2p, Fe 2p, and O 1s peaks. The ratio of the peaks area corrected by the atomic and instrument sensitivity factors yield an average surface composition of $Si_8O_{16}Fe$ for the aged Fe-SiNPs. Comparison of the surface Fe:Si ratio (1:8) with the Fe:Si bulk composition of the particles (1:4) determined from ICP- AES analysis, indicates a higher Fe content in the particle core. The iron content in the SiNPs is significantly higher than that expected for the Fe:Si molar ratio used in the initial mixture of the synthesis procedure (1:190). This behavior might be a consequence of the favored crystallization of Fe-SiNPs by iron, in line with theoretical studies on Si_nFe clusters with $n \leq 24$.[12] These studies predict that the silicon cluster stability is increased due to Fe content, though stability gradually decreases with increasing number of Fe atoms.[12-14] Moreover, the center site was found to be the most energetically preferred substitution site.

Si 2p and 2s XPS peaks (see Figure 2) show the contributions of Si^o (99.0 and 150.9 eV, respectively) and Si^{2+} (101.6 and 153.1 eV, respectively) environments. Silicon oxidation is further supported by the O 1s peak contribution at 532.2 eV (94% of total O) assigned to $Si(O-)_x$ environments.[15] The Fe 2p3/2 and Fe 2p1/2 main line peak positions at 710.6 and 724.0 eV (see Figure 2) and the signals separation, ΔE (BE 2p3/2 − BE 2p1/2), of about 13.5 eV agrees well with literature values for iron oxides,[15-17] as also supported by the O 1s band at 529.8 eV characteristic of Fe-oxides.[18] Deconvolution of the Fe 2p region (see Figure 2) was best optimized considering the contribution of three principal peaks, one shake up satellite, and one set of non-monochromatic front satellite to 8.4 eV at low BE from each peak. The fitting considers a Tougaard background line type and the Auger oxygen signal O KLL at higher BE The

peak at 710.5 eV (48% of total iron) due to Fe^{2+}/Fe^{3+} oxidation states supports magnetite formation while that at 714.7 eV (23% of total iron) is characteristic for Fe^{3+} oxidation states.[16, 17] In fact, the satellite band at 718.9 eV further supports the presence of Fe^{3+} oxidation states as γ-Fe_2O_3. Also, a very small peak (2.6% of total iron) at 707.2 eV due to either Fe^{o} or iron silicide is observed.[19] The obtained results support Fe^{3+} partial reduction to Fe^{2+} during synthesis[20] as well as the coexistence of Fe^{2+}/Fe^{3+} oxides. Since XPS surface sampling extends to depths of about a few nanometers depending on the emitted electron energies and density of the upper layers,[21] a great part of the 2-4 nm size particle volume is being sampled by this technique. Therefore, Fe/Si phases of SiO_x-Fe-SiNPs particles core comprise mainly iron oxides, iron ions, and silicon.

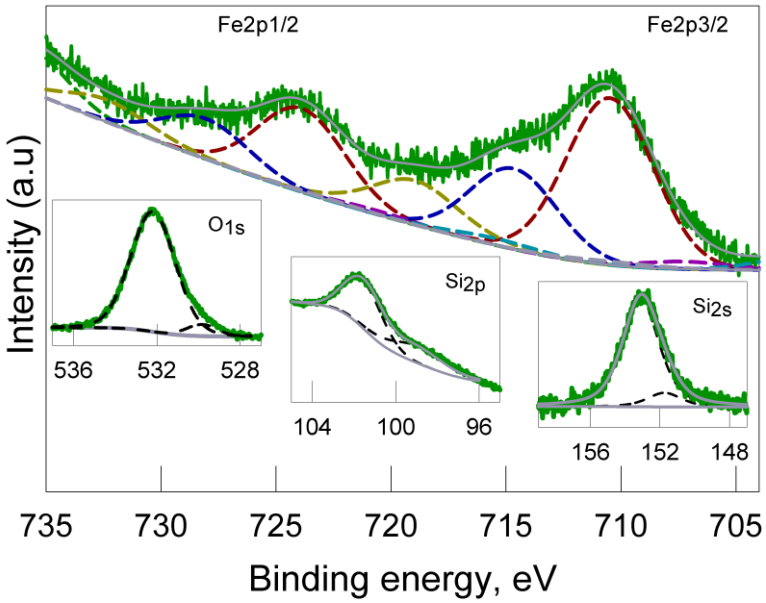

Figure 2: Si 2p, Si 2s, O 1s, and Fe 2p XPS peaks of SiO_x-Fe-SiNPs.

Figure 3 (A) shows, from top to bottom, the FTIR spectra of PA-SiNPs and PA-Fe-SiNPs. The PA-SiNPs spectrum shows characteristic absorption peaks due to primary amines at 1100–1250 and 1650 cm^{-1} due to C-N stretching and scissoring, respectively, as well as absorption at 660 cm^{-1} due to NH wagging. The presence of

bands at 1435 and 1250 cm^{-1} due to Si-C vibrations, as well as the peaks in the 2945–2880 cm^{-1} region due to CH_2 stretching and bending support the covalent bonding of PA to SiNPs.[22] Surface oxidation of the particles has to be taken into account since the peak at 1110 cm^{-1} may also show some contribution of the bands at 1150 and 1040 cm^{-1} identifying the presence of Si-O-Si.

On the other hand, the PA-Fe-SiNPs FTIR spectrum shows bands due to Fe–O stretching vibrations in the 630–580 cm^{-1} range.[23] The vibrational bands at 584 cm^{-1} are assigned to the Fe–O–Si bond which is in agreement with the broad signal at 950 cm^{-1}, revealing the presence of the Si–O group. The absence of a band at 1112 cm^{-1} assigned to the Si-O-Si group supports a low degree of SiNPs oxidation. Broad bands at 3000, 2450, 2080, and 1630 cm^{-1} are characteristic of primary amine salts and are assigned to NH_3^+ stretching and deformation combinations.[24] The band at 2775 cm^{-1} is attributed to N-CH stretching in amine salts. The presence of bands at 1430–1460 cm^{-1} due to Si-C vibrations and the peaks in the 2945–2800 cm^{-1} region due to CH stretching vibrations in amine salts corroborates the formation of covalent PA bonds at the Fe-SiNPs surface.

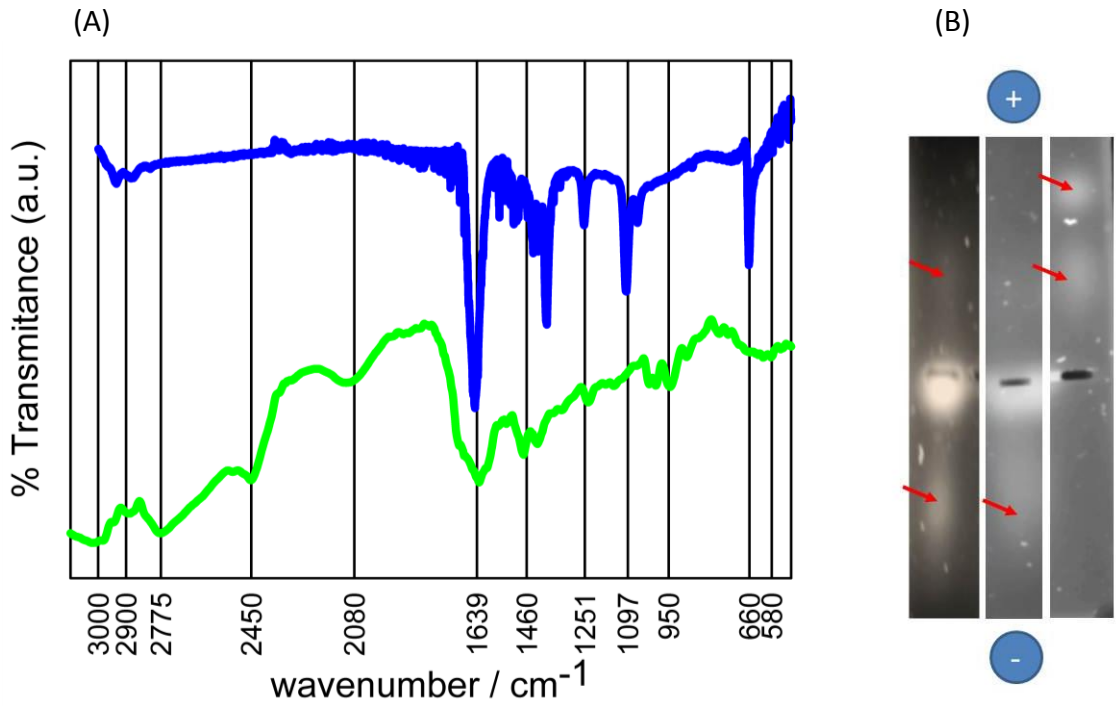

Figure 3: (A) FTIR spectra of PA-SiNPs (top blue spectrum) and PA-Fe-SiNPs (green bottom spectrum). The vertical solid lines serve as guide line for the eye. (B) Agarose gel electrophoresis of (from left to right) SiO_x-Fe-SiNPs, PA-Fe-SiNPs, and a negatively charged reference.

The gel electrophoresis experiments using 1% agarose gels in TAE buffer of pH 8 (see Figure 3 (B)) clearly demonstrate that the PA-Fe-SiNPs move faster toward the negative electrode which is expected for positively charged surface NH_3^+ groups. In comparison with it, SiO_x-Fe-SiNPs are composed of predominantly positively charged surface groups and a smaller fraction carrying negatively charged surface groups. Since mainly negatively charged SiO^- groups are expected for surface oxidized SiNPs at pH 8, the latter observations might suggest the contribution of iron to the overall surface charge. In fact, iron oxides are amphoteric solids that may provide charges due to the protonation and de-protonation reactions of Fe-OH surface sites (Fe-OH + H^+ ⇔ Fe-OH_2^+ and Fe-OH ⇔ Fe-O^- + H^+, respectively) with a surface charge reversal at pH ~ 8.[25, 26] The significant contribution of surface iron may explain both, the running direction and the low mobility of SiO_x-Fe-SiNPs in suspensions of pH 8.

Photoluminescence measurements. The excitation wavelength dependence of the PL emission spectrum of aqueous suspensions of PA-SiNPs, SiO_x-SiNPs, PA-Fe-SiNPs, and SiO_x-Fe-SiNPs strongly suggests the contribution of SiNPs with different size, morphology, and surface chemistry. The contribution of different emitters to the overall PL excitation-emission contour plot was analysed on the assumption that the SiNP suspensions comprises distinct, individual chromophores exhibiting excitation wavelength-invariant PL emission spectra. Figure 4 shows the excitation and emission spectra of the minimum number of contributing emitters to the overall PL as obtained from the bilinear analysis of the PL excitation-emission matrix (PL-EEM) of aqueous

suspensions of each SiNP sample. Namely, ***a'*** and ***b*** represent the contributing emitters to the PL-EEM of SiO_x-SiNPs, ***a"*** and ***c*** to that of PA- SiNPs, ***a"'*** and ***d*** to that of PA-Fe-SiNPs, and ***a""***, ***e***, and ***f*** to that of SiO_x-Fe-SiNPs.

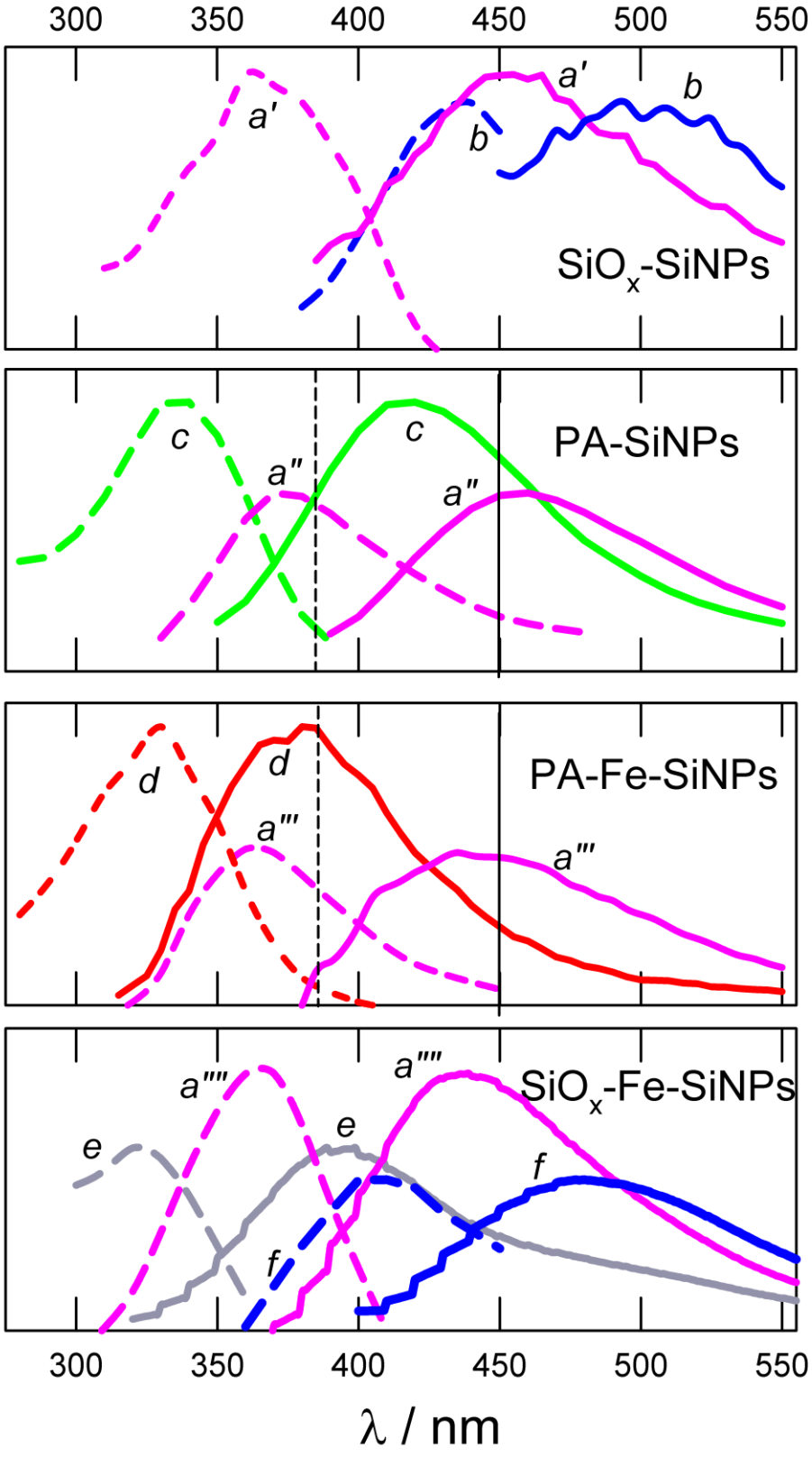

Figure 4: PL emission (solid lines) and PL excitation (dashed lines) spectra at 298 K of aqueous suspensions of contributing emitters as obtained from the bilinear analysis of the PL-EEM of SiO_x-SiNPs (***a'*** and ***b***), PA-SiNPs (***a"*** and ***c***), PA-Fe-SiNPs (***a"'*** and ***d***), and SiO_x-Fe-SiNPs (***a""***, ***e***, and ***f***). The vertical lines highlight the PL excitation (dashed line) and detection (full line) wavelengths used in time-resolved experiments.

The mean energy gap (EG) of charge carriers was evaluated for each individual contributing species using the PL excitation spectrum threshold.[22] The EG and the Stokes shift (SS) of the different contributing emitters are depicted in Table 1. It should be noted that when more than two contributing species are present as in the case of the PL-EEM of SiO_x-Fe-SiNPs, the bilinear analysis yields autoconsistent solutions of the problem. Thus, it results extremely difficult to obtain with precision the real excitation and emission spectra of the individual contributing species without additional external information.[27] Consequently, the EG of species ***a""***, ***e***, and ***f*** were not evaluated.

Particle	Species	**EG** (± 0.07)/ eV	λ_{em}^{max} (± 0.05)/eV	**SS** (± 0.05)/ eV	**τ(%)** / ns	*D*/ nm
PA-SiNPs	*a"*	2.69	2.74	0.62	1.9(60) 4.8 (37) 16 (3)	1.9
	c	3.22	3.0	0.74	ND	1.5-1.6
PA-Fe-SiNPs	*a"'*	2.82	2.80	0.60	1.1 (50) 3.8 (44) 10 (6)	1.8
	d	3.23	3.27	0.49	ND	1.5-1.6
SiO_x-SiNPs	*a'*	2.83	2.75	0.65	ND	1.8
	b	----	2.45	0.40		----
SiO_x-Fe-SiNPs	*a""*	----	2.82 (± 0.1)	0.5 (± 0.14)	ND	----
	e	----	3.2 (± 0.1)	0.7 (± 0.14)		
	f	----	2.55 (± 0.1)	0.5 (± 0.14)		

Table 1: Energy gap (EG), maximum PL emission (λ_{em}^{max}), Stokes shifts (SS), and decay times (τ) of the contributing species to the overall emission of the particles

suspensions obtained at 298 K. *D* stands for the average diameter of the particles as predicted from theoretical correlations according to the work of Delley et al.[28] ND stands for "not determined".

The PL excitation-emission spectra (including EG, λ_{em}^{max}, and SS) of emitting species ***a'***, ***a", a"',*** and ***a""***, are comparable within the experimental error and may therefore be assigned to the same contributing species, hereafter denoted as ***a***. The EG values are coincident with the PL maximum and thus, confirm that the PL excitation and emission spectra of species ***a*** originate from the same optical transitions.

The luminescent species ***c, d***, and ***e*** show comparable excitation spectrum and EG values (except for the unknown EG of ***e***), yet their PL emission spectrum, and consequently their SS, are not coincident (see Table 1). These observations suggest a unique excitation transition leading to exciton formation and its further relaxation to different lower-lying emitting states originated from different defects introduced by N, O, and Fe. On the other hand, the excitation and emission spectra of species ***b*** and ***f*** are, within the experimental error, coincident. Therefore, ***b*** and ***f*** are assigned to the same emitting species contributing solely to the PL-EEM of surface oxidized particles. From the previous discussion, it appears that Fe affects SiNPs PL-EEM through the introduction of low-lying emitting states and by PL quenching.

The values of the average SiNP sizes determined from the measured EG values upon assuming the effective mass model do not coincide with those estimated from TEM micrographs (see Table 1).[28] Therefore, time-resolved PL anisotropy experiments of aqueous suspensions of PA-Fe-SiNPs at 298 K were carried out to obtain complementary information of SiNP sizes. PL anisotropy measurements were performed by exciting species ***a*** at 388 nm and detecting the PL at 450 nm. The PL

anisotropy decay could be well fitted to a single exponential function, $r(t) = r_0 \times \exp(t/\theta)$, which confirms the spherical shape of the emitting SiNPs. As best-fit parameter the values for the intrinsic anisotropy and the rotational correlation time, with $r_0 = 0.35$ and $\theta = 0.85$ ns, were obtained. The non-zero value of the intrinsic anisotropy clearly reflects the difference in the orientation of ground-state and excited-state dipole moments, which is in agreement with the observed large Stokes shifts. Using the value of the shear viscosity of water at 25°C, 0.0091 poise, and $\theta = 0.85$ ns, the mean size of the species ***a*** can be determined to be 2.0 nm. Since HR-TEM images in Figure 1 demonstrate that the most abundant SiNPs have sizes in the range of 3.8-4.8 nm, the mean size of 2.0 nm determined from the PL anisotropy experiments might indicate that smaller SiNPs exhibit more intense PL than larger ones.[29] The latter result is further supported by calculated mean sizes from theoretical correlations.[28]

The PL decay times, τ, of species ***a*** were obtained from tri-exponential decay fittings of the PL traces detected at 450 nm upon 388 nm excitation (see in Table 1). For the PA-Fe-SiNP samples the time constants of the species ***a***, with $\tau_1 = 1.1$ ns, $\tau_2 = 3.8$ ns, and $\tau_3 = 10$ ns, are significantly shorter than those obtained for the PA-SiNP sample. This result nicely proves that incorporated Fe atoms or surface-adsorbed Fe^{3+} ions efficiently quench the SiNP PL due to both, a dynamic and static quenching process (see S.I. – Fe^{3+} quenching).

Singlet oxygen generation. Singlet Oxygen formation upon 355 nm irradiation of SiO_x-Fe-SiNPs suspensions in toluene is evidenced by the time-resolved phosphorescence traces observed at 1270 nm (Figure 5 *inset A*). From the comparison of the total $^1O_2$ phosphorescence emission generated by the SiO_x-Fe-SiNPs (I_Δ) and that generated by the DPA reference ($I_{\Delta R}$) under similar solution absorbance (A) at 355 nm and experimental setup, and taking $\Phi_{\Delta R} = 0.8$ for the reference in toluene,[30] a quantum

yield of $^1O_2$ generation $\Phi_\Delta = 0.06 \pm 0.01$ is obtained. The latter value is smaller than that of iron-free surface-oxidized SiNPs in toluene suspensions,[2] thus indicating a non-negligible effect of iron in the generation capacity of $^1O_2$. The fitting of $^1O_2$ traces to an exponential decay $I_{1O2}(t) = I_{1O2}(t=0)\times\exp(-t/\tau_\Delta)$ with I the phosphorescence intensity (see fitting curves in Figure 5) yields the $^1O_2$ lifetime, τ_Δ. Singlet oxygen lifetimes of 10, 25, and 26.9 μs were obtained in toluene suspensions of SiO_x-Fe-SiNPs, SiO_x-SiNPs, and in toluene solutions of DPA in the absence of quenchers, respectively (see ref. 8 and traces in Figure 5 and *inset* A). Therefore, these observations indicate an effective $^1O_2$ quenching by SiO_x-Fe-SiNPs, which may be attributed to the incorporation of Fe. To demonstrate the $^1O_2$ quenching ability of SiO_x-Fe-SiNPs, experiments were performed in which $^1O_2$ was generated upon 355 nm irradiation of DPA in toluene solutions in the presence of SiO_x-Fe-SiNPs. Faster decays of $^1O_2$ phosphorescence, and therefore decreasing τ_Δ, were observed in the presence of increasing [SiO_x-Fe-SiNPs] (see Figure 5). The slope of the straight line of τ_Δ^{-1} *vs*. [SiO_x-Fe-SiNPs] shown in Fig. 5 *inset* B, yields the $^1O_2$ quenching rate constant $k_q = 0.6$ dm^3 g^{-1} s^{-1} for SiO_x-Fe-SiNPs. Moreover, the lower $I_{1O2}(t=0)$ values obtained in experiments in the presence of SiO_x-Fe-SiNPs compared to those in their absence (see Figure 5) indicates a diminution in the quantum yield of $^1O_2$ generation due to specific interactions of DPA and SiO_x-Fe-SiNPs, as supported by the changes observed in the absorption spectrum of DPA in the presence of increasing [SiOx-Fe-SiNPs].

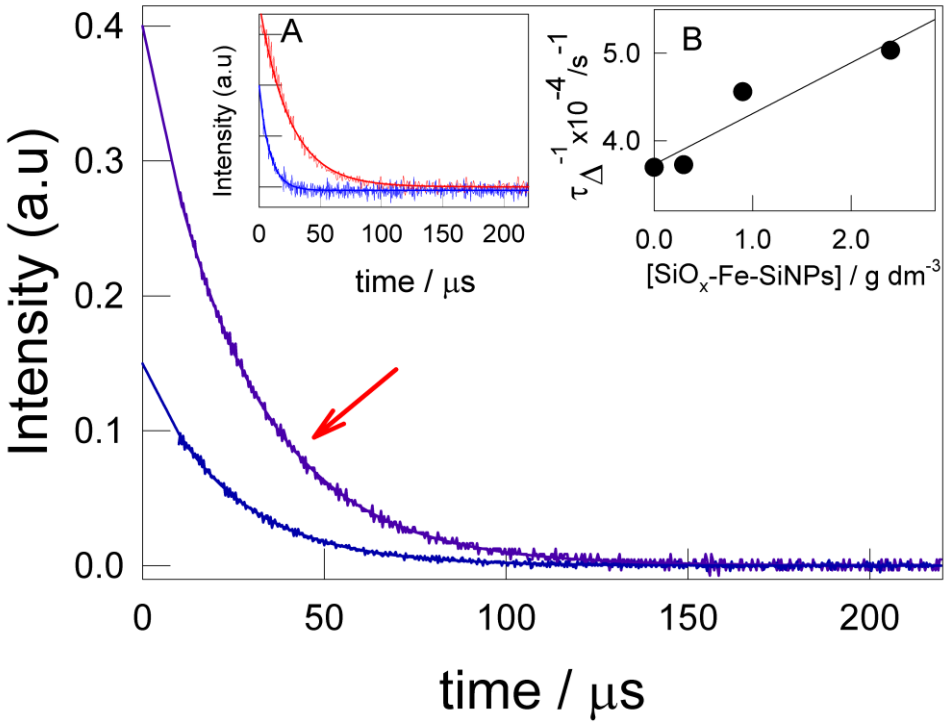

Figure 5: Singlet oxygen phosphorescence decay curves at 1270 nm obtained upon 355 nm excitation of DPA in air-saturated toluene solution (upper curve) and after addition of SiO_x-Fe-SiNPs (lower curve). Full lines stand for the curve fitting to a single exponential decay. *Inset* A: Singlet oxygen phosphorescence at 1270 nm obtained upon 355 nm excitation of SiO_x-Fe-SiNPs (lower curve) and SiO_x-SiNPs (upper curve) suspensions in toluene. *Inset* B: Plots of τ_Δ^{-1} *vs.* [SiO_x-Fe-SiNPs].

On the other hand, no $^1O_2$ phosphorescence emission was observed in analogous experiments performed with PA-Fe-SiNPs and PA-SiNPs suspensions in toluene. Considering that both particles types are functionalized with NH groups, the lack of observation of $^1O_2$ phosphorescence may be assigned to an efficient quenching by surface NH groups, which prevent the detection of $^1O_2$ phosphorescence emission in the microsecond time range. In fact, the generation and strong quenching of $^1O_2$ by PA-SiNPs obtained from a wet chemical procedure was demonstrated in the literature using continuous irradiation scavenging experiments.[31]

Cell viability. The cytotoxicity of Fe-SiNPs towards C6 cells was determined by the MTT assay.[32] Figure 6 shows C6 cells viability after 24h exposure to different concentrations of SiO_x-Fe-SiNPs and PA-Fe-SiNPs. Exposure to 10 µg/ml of SiO_x-Fe-SiNPs and PA-Fe-SiNPs resulted in 5% and 15% decrease of cell viability, respectively. 100 µg/ml of SiO_x-Fe-SiNPs induced a 35% of cell death while PA-Fe-SiNPs at the same concentration are highly cytotoxic causing an 85% decrease of cell viability.

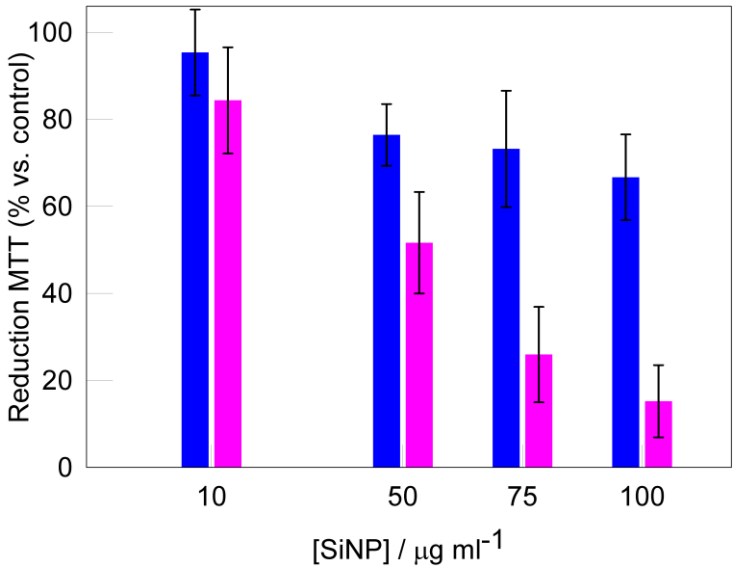

Figure 6: MTT assays on C6 cells after 24h exposure to different concentrations of (■) SiO_x-Fe-SiNPs and (■) PA-Fe-SiNPs.

These observations agree satisfactorily with reported cytotoxicity studies of SiNPs with surface attached amino groups.[33] Since in aqueous media of pH 7-8 both, PA-Fe-SiNPs and SiO_x-Fe-SiNPs are positively charged, it is suggested that the nature of the charge, $-NH_3^+$ *vs* $Fe–OH_2^+$ is a contributing factor to the differential cell toxicity.

CONCLUSIONS

Water-soluble Fe-containing SiNPs were synthesized via the high temperature reaction of a solid mixture containing Si, Na and $Fe(acac)_3$ yielding the NaSi precursor

that contains Fe atoms. Subsequently, the Fe-doped NaSi precursor reacts with NH_4Br which produces hydrogen-terminated Fe-SiNPs which were either, gently surface oxidized or further terminated with allylamine via photochemical hydrosilylation to yield positively charged surfaces. The synthesis procedure leads to the generation of two different types of SiNPs. Fe-containing SiNPs were found to exhibit high density and a lattice spacing of 2.1 ± 0.1 Å resembling the (400) spacing in cubo-octahedral morphologies of botanical magnetite. In particular, the surface and bulk Fe:Si molar ratios were observed to be significantly higher than the analytical ratio used in the synthesis procedure. This clearly indicates that crystallization of Fe-SiNPs with high Fe contents is favored. In addition, the partial reduction of Fe(III) to Fe(II) during synthesis takes place.

Furthermore, incorporation of iron significantly decreases the PL quantum yields and PL lifetimes of SiNPs. PL anisotropy experiments indicate that iron-free SiNPs with sizes < 2 nm exhibit intense PL and thus, were shown to contribute with a larger proportion to the overall PL than the larger-sized population of particles observed by HR-TEM. Fe-containing SiNPs were observed to produce $^1O_2$, and the $^1O_2$ quenching by the particles was found to strongly depend on the nature of the surface groups. Cytotoxicity studies using MTT assay of SiNPs internalized by rat glioma C6 cells also indicate a strong dependence of the SiNP cytotoxicity on the nature of the surface groups. In particular, 100 µg/ml of PA-Fe-SiNPs lead to 85% decrease in cell viability while equal amounts of SiO_x-Fe-SiNPs induced a 35% of cell death.

ACKNOWLEDGMENT

J.J.R. and C.R.L. thank Consejo Nacional de Investigaciones Científicas y Técnicas (CONICET, Argentina) for a graduate studentship. M.C.G., M.L.K., A.R. and H.B.R. are research members of CONICET, Argentina. This research was supported by

the grant PIP 112-200801-00356 from CONICET. The authors thank DAAD (PROALAR 54365954, Germany) and MINCYT (Argentina) for a collaboration project. Support of the Deutsche Forschungsgemeinschaft (graduate school 1161/2) is gratefully acknowledged.

REFERENCES

(1) Burda, C.; Chen, X.; Narayanan, R.; El-Sayed, M. A., Chemistry and Properties of Nanocrystals of Different Shapes. *Chem. Rev.* **2005**, *105*, 1025-1102.

(2) Llansola Portolés, M. J.; David Gara, P. M.; Kotler, M. L.; Bertolotti, S.; San Román, E.; Rodríguez, H. B.; Gonzalez, M. C. Silicon Nanoparticle Photophysics and Singlet Oxygen generation. *Langmuir* **2010**, *26*, 10953 - 10960.

(3) Liang, S.; Islam, R.; Smith, D. J.; Bennett, P. A.; O'Brien, J. R.; Taylor, B. Magnetic Iron Silicide Nanowires on Si (110). *Appl. Phys. Lett*. **2006**, *88*, 113111 - 113114.

(4) Erogbogbo, F.; Yong, K.-T.; Hu, R.; Law, W.-Cheung; Ding, H.; Chang, C.-W.; Prasad, P.N.; Swihart, M.T. Biocompatible Magneto-fluorescent Probes: Luminescent Silicon Quantum Dots Coupled with Superparamagnetic Iron(III) Oxide. *ACS Nano*, **2010**, *4*, 5131 - 5138**.**

(5) Sato, K.; Yokosuka, S.; Takigami, Y.; Hirakuri, K.; Fujioka, K.; Manome, Y.; Sukegawa, H.; Iwai, H.; Fukata, N. Size-Tunable Silicon/Iron Oxide Hybrid Nanoparticles with Fluorescence, Superparamagnetism, and Biocompatibility. *J. Am. Chem. Soc.* **2011**, *133*, 18626 - 18633.

(6) Singh, M. P.; Atkins, T. M.; Muthuswamy, E.; Kamali, S.; Tu, C.; Louie, A. Y.; Kauzlarich, S. M. Development of Iron-Doped Silicon Nanoparticles As Bimodal Imaging Agents. ACS *Nano* **2012**, *6*, 5596 - 5604.

(7) Lakowicz, J. R. Principles of Fluorescence Spectroscopy, 3rd ed.; Springer, Singapore, **2006**.

(8) Wilkinson, F.; Helman, W. P.; Ross, A. B. Rate Constants for the Decay and Reactions of the Lowest Electronically Excited Singlet State of Molecular Oxygen in Solution. An Expanded and Revised Compilation. *J. Phys. Chem. Ref. Data* **1995**, *24*, 663 - 1021.

(9) Llansola Portolés, M. J.; Pis Diez, R.; Dell'Arciprete, M. L.; Caregnato, P.; Romero, J. J.; Mártire, D. O.; Azzaroni, O.; Ceolín, M.; Gonzalez, M. C. Understanding the Parameters Affecting the Photoluminescence of Silicon Nanoparticles. *J. Phys. Chem. C* **2012**, *116*, 11315- 11325.

(10) Gajdardziska, M.; McClean, R.G.; Schofield, M.; Sommer, C.V.; Kean, W.F. Discovery of Nanocrystaline Botanical Magnetite. *Eur. J. Mineral.* **2001**, *13*, 863–870.

(11) Collingwood, J. F.; Chong, R. K. K.; Kasama, T.; Cervera-Gontard, L.; Dunin-Borkowski, R.E.; Perry, G.; Posfaig, M.; Siedlak, S. L.; Simpson, E.T.; Smith, M.A.; et al. Three-Dimensional Tomographic Imaging and Characterization of Iron Compounds within Alzheimer's Plaque Core Material. *J. Alzheimer's Dis.* **2008**, *14*, 235–245.

(12) Mahtout, S. Effect of Iron Atoms on the Properties of Silicon Cage Clusters. *Acta Phys. Polonica A* **2013**, *124*, 688 – 694.

(13) Mahtout, S.; Belkhir, M.A. Structural, Magnetic and Electronic Properties of Fe Encapsulated by Silicon Clusters. *Physics Letters A* **2006**, *360*, 384–389.

(14) Ma, Li; Zhao, J.; Wang, Ji.; Wang, B.; Wang, G. Magnetic Properties of Transition-Metal Impurities in Silicon Quantum Dots. *Phys. Rev. B* **2007**, *75*, 045312

(15) NIST X-ray Photoelectron Spectroscopy Database, Version 4.1 (National Institute of Standards and Technology, Gaithersburg, 2012); http://srdata.nist.gov/xps/.

(16) Yamashita, T.; Hayes, P. Analysis of XPS Spectra of Fe^{2+} and Fe^{3+} ions in Oxide Materials. *Appl. Surf. Sci.* **2008**, *254*, 2441–2449.

(17) Claessen, R.; Sing, M.; Paul, M.; Berner, G.; Wetscherek, A.; Müller, A.; Drube, W. Hard X-Ray Photoelectron Spectroscopy of Oxide Hybrid and Heterostructures: a New Method for the Study of Buried Interfaces. *New J. Phys.* **2009**, *11*, 125007 - 125023.

(18) Biesinger, M.C.; Payne, B.P.; Grosvenor, A.P.; Lau, L.W.M.; Gerson, A.R.; Smart, R. St.C. Resolving Surface Chemical States in XPS Analysis of First Row Transition Metals, Oxides and Hydroxides: Cr, Mn, Fe, Co and Ni. *Appl. Surf. Sci.* **2011**, *257*, 2717–2730.

(19) Ohtsu, N.; Oku, M.; Satoh, K.; Wagatsuma, K. Dependence of Core-Level XPS Spectra on Iron Silicide Phase. *Appl. Surf. Sci*. **2013**, *264*, 219 - 224.

(20) Li, P.; Jiang, E. Y.; Bai, H. L. Fabrication of Ultrathin Epitaxial γ-Fe_2O_3 Films by Reactive Sputtering. *J. Phys. D: Appl. Phys.* **2011**, *44*, 75003-75008.

(21) Cumpson, P. J.; Seah, M. P. Elastic Scattering Corrections in AES and XPS. II. Estimating Attenuation Lengths and Conditions Required for Their Valid Use in Overlayer/Substrate Experiments. *Surf. Interface Anal.***1997**, *25*, 430−446.

(22) Romero, J. J.; Llansola-Portolés, M. J.; Dell'Arciprete, M. L.; Rodríguez, H. B.; Moore, A. L.; Gonzalez, M. C., Photoluminescent 1–2 nm Sized Silicon Nanoparticles: A Surface-Dependent System. *Chem. Mater*. **2013**, *25*, 3488-3498.

(23) Corr, S.A.; Gun'ko, Y.K.; Douvalis, A.P.; Venkatesan, M.; Gunning, R.D.; Nellist, P.D. From Nanocrystals to Nanorods: New Iron Oxide-Silica Nanocomposites from Metallorganic Precursors. *J. Phys. Chem. C* **2008**, *112*, 1008-1018.

(24) Lin-Vien, D.; Colthup, N. B.; Fateley, W. G.; Grasselli, J. G. The Handbook of Infrared and Raman Characteristic Frequencies of Organic Molecules. Elsevier, **1991**.

(25) Tombacz, E.; Majzik, A.; Horvát, ZS.; Illés, E. Magnetite in Aqueous Medium: Coating its Surface and Surface Coated with it. *Romanian Rep. Phys.* **2006**, *58*, 281–286.

(26) Lucas, I.; Durand-Vidal, S.; Dubois, E.; Chevalet, J.; Turq, P. Surface Charge Density of Maghemite Nanoparticles: Role of Electrostatics in the Proton Exchange. *J. Phys. Chem. C* **2007**, *111*, 18568 – 18576.

(27) San Román, E.; Gonzalez, M.C. Analysis of Spectrally Resolved Kinetic Data and Time-Resolved Spectra by Bilinear Regression. *J. Phys. Chem.* **1989**, *93*, 3532-3536.

(28) Delley, B.; Steigmeier, E. F. Size Dependence of Band Gaps in Silicon Nanostructures. *Appl. Phys. Lett.* **1995**, *67*, 2370.

(29) Smith, A.; Yamani, Z. H.; Roberts, N.; Turner, J.; Habbal, S. R.; Granick, S.; Nayfeh, M. H. Observation of Strong Direct-Like Oscillator Strength in the Photoluminescence of Si Nanoparticles. *Physical Review B* **2005**, *72*, 205307.

(30) Wilkinson, F; Helman, W. P.; Ross, A. B. Quantum Yields for the Photosensitized Formation of the Lowest Electronically Excited Singlet State of Molecular Oxygen in Solution. *J. Phys. Chem. Ref. Data* **1993**, *22*, 113-262.

(31) Lillo, C.R.; Romero, J.J.; Llansola Portolés, M.J.; Pis Diez, R.; Caregnato, P; Gonzalez, M.C. Organic-Coating of 1-2 nm Size Silicon Nanoparticles: Effect on the Particle Properties. *Nano Res.* **2015**. DOI 10.1007/s12274-015-0716-z.

(32) Alaimo, A.; Gorojod, R.M.; Beauquis, J.; Muñoz, M.J.; Saravia, F.; Kotler, M.L. Deregulation of Mitochondria-Shaping Proteins Opa-1 and Drp-1 Plays a Decisive Role in Manganese-Induced Apoptosis. *PLOS One* **2014**, *9*, e91848.

(33) Bhattacharjee, S.; de Haan, L.H.; Evers, N.M.; Jiang, X.; Marcelis, A.T.; Zuilhof, H.; Rietjens, I.M.; Alink, G.M. Role of Surface Charge and Oxidative Stress in

Cytotoxicity of Organic Monolayer-Coated Silicon Nanoparticles Towards Macrophage NR8383 Cells. *Part Fibre Toxicol.* **2011**, *7*, 25-32.

Supporting Information Available: Fe^{3+} quenching experiments of SiNPs fluorescence. This material is available free of charge via the Internet at http://pubs.acs.org.

TOC Graphics